Journal of Geosciences, Osaka City University
Vol. 49, Art. 8, p. 137-151, March, 2006

Continental Growth of Bastar Craton, Central Indian Shield during Precambrian via Multiphase Subduction and Lithospheric Extension/Rifting: Evidence from Geochemistry of Gneisses, Granitoids and Mafic dykes

M. E.A. MONDAL[1]*, M. Faruque HUSSAIN[1,2] and T. AHMAD[3]

[1] Department of Geology, AMU, Aligarh- 202002, India
[2] Present Address: Department of Geology, Mizoram University, Aizwal-796007, India
[3] Department of Geology, University of Delhi, New Delhi -110007, India
E-Mail: emondal2002@yahoo.co.in

Abstract

Two major tectono-magmatic episodes can be recognized within Bastar craton. The first episode is represented by granitic-gneisses and the second one is represented by bi-modal granitoids-basic magmatic events. The multi-element patterns for the gneisses are fractionated (LILE enriched, HFSE depleted) with negative anomalies at P and Ti. REE patterns are moderately to highly fractionated (La_N/Yb_N = 8 - 51). The gneisses have calc-alkaline trend, K/Rb ratios ranging from 117 to 325 (average 225) and the Rb/Sr values averaging 0.9. These geochemical features coupled with average concentration of Y (23ppm), Nb (17ppm), Rb (145ppm) and Th (31ppm) of the Bastar gneisses indicate an arc related tectonic setting for the protoliths. In general the geochemistry of the granitoids shows resemblance with that of the gneisses in terms of their fractionated multi-element patterns (elevated LILE in comparisons to the HFSE with strong depletion at P and Ti) and also points to volcanic arc tectonic setting. Two groups of mafic dykes are recognized within the craton; one is metamorphosed amphibolites while the other is unmetamorphosed dolerites. The geochemical features of the dolerites indicate contamination of the mantle source by sediment, whereas those of the amphibolites have been interpreted to represent variations in source characteristics in the underlying mantle. Our study indicates change in the nature of subduction related magmatism from dominantly felsic during Archaean to bimodal (acidic-basic) magmatism during Proterozoic as observed in many well-studied terrains all over the world.

Key-words : Bastar Craton, Central India, Geochemistry, Gneisses, Granitoids, Mafic dykes, Precambrian crustal evolution

1. Introduction

To understand the formation and growth of the continental crust through geologic time, it is most important to study the rocks viz. tonalite-trondhjemite-granodiorite (TTG), gneisses, granulites, greenstone belts and calc-alkaline granitoids that constitute the bulk of most of the Archaean cratons. The Bastar craton in the Central Indian shield consists dominantly of Archaen granitic gneisses and granitoids. These rocks provide an excellent opportunity to study the origin of these rocks and their role in the formation and evolution of the continental crust in the Bastar craton. The gneisses are dominantly of granitic composition. However, granitic gneisses of trondhjemitic affinities are also present, although their occurrences are

restricted in the southern Bastar. These trondhjemitic gneisses occur as enclaves within the granitoids (Sarkar, G. et al., 1993). The granitoids contain enclaves of gneisses, indicating that the granitoids are younger than the gneisses. The un-deformed nature of the granitoids may indicate that the craton attained stability after the emplacement of the granitoids and no further orogenic movements occurred subsequently. Mafic dykes and dyke swarms, emplaced along dominantly NW - SE direction, represent the mafic magmatic event. The dykes belong principally to two distinct groups: un-metamorphosed dolerites and amphibolites. Based on field evidence, the amphibolites are considered older and the dolerites are younger.

The pioneering work on the craton was done by Crookshank (1963) who mapped the craton and classified the rock suites into stratigraphic successions. Subsequently many earth scientists have worked on different aspects including structure, tectonics, magmatism and geochronology (Mishra et al., 1984; Sarkar A. et al., 1990; Sarkar G. et al., 1993; Srivastava et al., 1996; Asthana et al., 1996; Neogi et al., 1996), but comprehensive works on the petrological and geochemical aspects of the gneisses, granitoids and the mafic dykes of the craton are lacking. The purpose of this paper is to constrain the possible petrogenetic mechanisms of the gneisses, granitoids and mafic dykes and further to understand the progressive changes in the nature of magmatism from dominantly felsic during Archaean to bimodal magmatism during Proterozoic.

2. Geological outlines

The Bastar craton lies south of the Narmada-Son-Lineament covering an area of approximately 2,15,000 km^2 within 17.5°N-23.5°N latitude and 77.8°E-84.1°E longitude (Fig.1). The Precambrian units of the craton are represented by gneisses, granitoids, metasedimentary supracrustals and mafic dykes which together make up the bulk of the geology of the Bastar craton. The older supracrustals (Archaean to Paleoproterozoic) consisting of quartzites, phyllites, mica schists, banded hematite quartzites and agglomerates, belong to Sausar, Sonakhan, Pakhal, Sukma, Bengpal, Bailadila, Nandgaon, Dongargarh, Khairagarh and Sakoli groups. The younger units of the craton are represented by the Gondwana Supergroup, Deccan Traps and undeformed sedimentary rocks of Meso- to Neoproterozoic age. These units consisting of shale, sandstone, conglomerate, limestone, dolomite etc. are contained in the rift related sedimentary basins of Chattisgarh, Indravati and Khariar within the

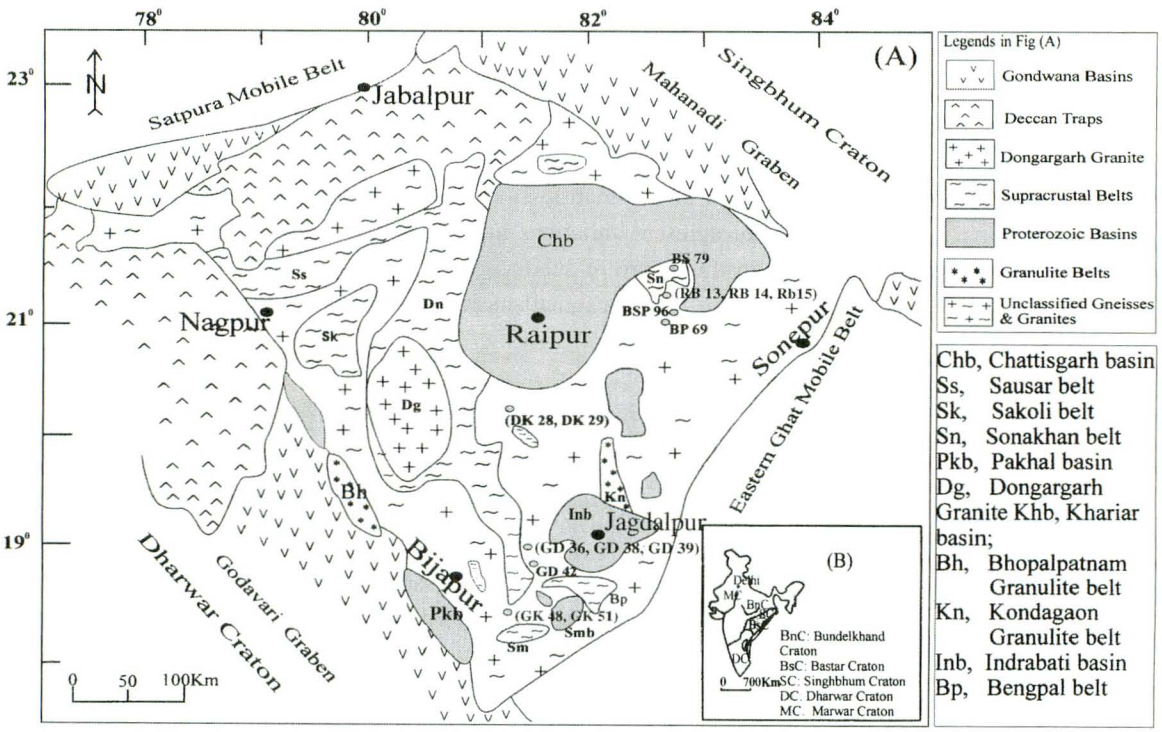

Fig. 1 Simplified geological map of Bastar craton, central India (after Ramakrishna, 1990). Inset: Geological map of India showing major Archaean cratons including Bastar (after Radhakrishna and Naqvi, 1986). Numbers refer to location of samples.

craton. These younger rocks cover the Precambrian formations of the craton over considerable areas particularly in the west, northwest and in the central part of the craton (Fig.1).

Granitic gneisses that occur as large outcrops are the most prominent and ubiquitous rock types of the craton and form the basement for the Precambrian metasedimentary supracrustals especially in the north, northwest and southern part of the craton. Gneisses also occur as enclaves within the granitoids of younger age in the southern Bastar region. These gneisses with high alumina contents and of trondhjemitic affinity have been dated at 3.5 Ga (Sarkar, G. et al., 1993). Granitoid plutons of varying dimensions occur as intrusives into the gneisses and into the metasupracrustals throughout the craton. The granitoids form the second largest rock unit of the craton. Xenoliths of gneisses and metasupracrustals abundantly occur within the granitoids. The mafic dykes and dyke swarms cut across all the older units along predominantly NW - SE direction. At places the dykes are overlain by the younger sedimentary formations over considerable distances. The dykes are approximately 20-200m wide and are 1-20 km long and exhibit a sharp contact with the country rocks. Petrographically the dykes belong principally to two distinct groups: (i) unmetamorphosed dolerites characterized by porphyritic texture with coarse-grained feldspar phenocrysts and (ii) faintly metamorphosed amphibolites characterized by porphyroblastic texture with hornblende and plagioclase megacrysts.

The trondhjemitic granitic gneisses occurring as enclaves and the host granitoids that contain the gneisses have yielded U-Pb zircon ages of 3.5Ga and 2.4Ga respectively (Sarkar, G. et al., 1993); an age of 3.0Ga has also been reported for the gneisses of granitic composition (Sarkar, A. et al, 1990). However, no evidence favoring two distinct generations of gneisses have been observed during our field investigations. In the absence of any compelling field evidence in favor of two distinct generations of gneisses and overlapping radiometric dates above, we consider the gneisses of granitic composition and the gneisses of trondhjemitic composition as a single rock unit, even though the geochemical data of both the gneisses have minor variations in terms of both major and trace elemental concentrations (Hussain et al., 2004). No well constrained radiometric age data are available for the mafic dykes. Based on cross-cutting relationship of the dykes with the host granite gneiss which have been dated to be ~2.5 Ga to ~2.6 Ga (Sarkar et al., 1994), it is considered that both groups of dykes have been emplaced at the end-Archaean (Srivastava et al., 1996).

3. Geochemistry

Fresh rock samples of gneisses, granitoids and mafic dykes have been collected from north and northeastern, central and southwestern parts of Bastar craton (Fig. 1). Prior to geochemical analysis, the rocks were studied under the microscope and samples, which show least alteration effects, were selected for geochemical analysis. There were fourteen representative samples of the gneisses, thirteen granitoids and eleven mafic dykes samples.

3.1 Analytical techniques

Whole rock major and trace element analyses were carried out at Wadia Institute of Himalayan Geology (WIHG), Dehra - Dun. Major elements were determined on WD-XRF (Simens SRS 3000) using fused disks, and pressed powder pellets were used for trace elements. The accuracy (%RSD) for major and minor oxide is better than 5% and the precision is better than 1.5%. Accuracy for the trace elements is better than 12% and long-term precision for the trace elements is better than 10% (Saini et al., 1998). Twelve representative samples (four each of gneisses, granitoids and mafic dykes) covering the geochemical variations were selected for trace elements including REE analysis at National Geophysical Research Institute (NGRI), Hyderabad on ICP-MS using Parkin Elmer Sciex ELAN DRC-II machine following the procedure described by Balaram et al (1996). The results are found matching with those of XRF data of WIHG. The precision of ICP-MS REE data is <5% RSD for all REE. International standards of USGS (United States Geological Survey) and GSJ (Geological Survey of Japan) were used for calibration and testing of accuracy. Whole rock major and trace element data of the gneisses, granitoids and mafic dykes are presented in Table 1, Table 2 and Table 3 respectively.

3.2 Major and trace elemental geochemistry

3.2.1 Gneisses

The gneisses are highly siliceous ($71 \leq SiO_2 \leq 75\%$) averaging 71.5%. The Al_2O_3 concentration ($13 \leq Al_2O_3 \leq 15\%$) averages 14wt%. For most of the rock samples the Al_2O_3 contents are <15wt% at SiO_2 value of ≥ 70wt%; which is a characteristic feature of the low alumina trondhjemites of Barker and Arth (1976). The molar alumina saturation index (A/CNK) values for the gneisses ranges from 1.02 to 1.21 and the gneisses can be categorized as peraluminous. The gneisses are poor in ferromagnesian content (Fe_2O_3+MgO+TiO_2 = 3.19%) and have low Mg # [100xMg/(Mg+Fe)], averaging 29. In the

Table 1 Representative major (wt%) and trace (ppm) element analyses of Bastar gneisses.

Sample No	RB13*	RB14	RB15*	DK28	DK29*	GD36	GD38	GD39	GD42*	GK48	GK51	BP69	BS79	BSP96	Av.TTG+	Av.EnGn**	55***	60***	63***
SiO2	74.59	71.05	70.13	72.41	69.92	70.75	72.65	73.09	70.2	71.88	71.6	69.65	72.08	70.66	69.79	69.14	69.27	68.7	69.01
TiO2	0.15	0.19	0.27	0.14	0.16	0.19	0.2	0.12	0.23	0.22	0.16	0.6	0.17	0.36	0.34	0.41	0.43	0.43	0.45
Al2O3	13.15	14.45	15.25	13.88	14.49	15.44	13.93	13.84	14.45	13.93	14.49	12.76	14.21	15.36	15.56	15.49	15.81	15.81	15.59
Fe2O3t	1.72	1.98	3	1.84	2.1	2.34	2.32	1.43	1.99	1.9	1.6	6.15	2.02	2.52	3.12	3.38	3.6	3.6	3.54
MnO	0.02	0.03	0.03	0.02	0.03	0.06	0.03	0.03	0.02	0.02	0.03	0.12	0.02	0.02	0.05	0.025	0.03	0.03	0.03
MgO	0.34	0.42	0.66	0.37	0.47	0.59	0.47	0.3	0.59	0.38	0.37	1.03	0.31	0.57	1.18	0.63	0.67	0.67	0.71
CaO	1.38	2.14	2.44	1.15	1.75	1.62	0.92	1.26	2.1	1.76	1.37	0.9	0.89	1.7	3.19	2.73	2.45	2.45	2.72
Na2O	3.39	4.13	4.62	4.14	5.62	4.67	3.32	3.75	4.83	4.12	5.1	2.33	3.57	4.07	4.88	4.27	4.38	4.38	4.43
K2O	4.3	3.19	2.73	4.14	1.3	3.66	4.08	4.29	2.02	3.29	2.93	4.86	5.65	4.13	1.76	2.61	2.79	2.79	2.26
P2O5	0.03	0.06	0.08	0.02	0.02	0.06	0.08	0.03	0.03	0.02	0.03	0.11	0.01	0.04	0.13	0.12	0.13	0.13	0.12
LOI	0.02	2.15	0.66	1.36	2.36	0.37	1.89	1.32	2.37	1.02	2.13	1.32	0.65	0.31		0.91	0.68	0.68	0.66
Total	99.09	99.79	99.87	99.44	98.25	99.76	99.89	99.46	98.83	98.54	99.81	99.84	99.59	99.73	100	99.71	99.52	99.67	99.52
Mg#	28	30	30	29	31	33	29	29	37	28	32	25	23	31	43	27	–	–	–
Cu	1..34	16.7	2.33	36.2	1.7	6.6	56.5	19.6	1.23	32.5	17	29.6	7.2	7.2	–	–	NA	NA	NA
Ni	10.64	9	7.98	13.9	12.15	17.2	17	13.1	9.08	10.8	9.6	11	12.5	12.1	14	–	NA	NA	NA
Co	51.27	nd	4.96	nd	43.82	nd	nd	nd	33.84	nd	nd	nd	nd	nd	–	–	NA	NA	NA
Sc	2.24	4.4	3.58	1.5	5.93	4.5	3.1	1.3	2.73	2.4	2.1	13.1	5.5	7.4	–	–	NA	NA	NA
Zn	29.18	29.8	42.35	23	44.8	45.4	33.7	27.7	46.55	31.2	33.8	72.9	15.7	41.6	–	–	NA	NA	NA
Ga	13.94	17.2	17.63	19	23.86	19.5	19.8	14.8	18.14	16.8	18.8	14.8	17.3	17	–	–	NA	NA	NA
Pb	27.06	36	95.66	43	27.78	33	64	34	28.29	27	19	35	55	83	–	–	NA	NA	NA
Cr	13.11	292	288.34	335	11.91	378	331	317	6.52	305	322	332	481	412	29	–	NA	NA	NA
Th	7.8	3.9	12.98	18.8	18.77	16.2	49.3	25.9	45.73	41.6	5.4	29.8	128.7	121.3	6.9	–	NA	NA	NA
Rb	108.97	98	88.25	159	91.99	235	151	262	62.06	93	99	130	284	163	55	–	NA	NA	NA
U	1.72	3.4	4.43	6.3	12.68	7.5	11.9	9	2.41	3.8	3.2	3.3	17.4	13.4	1.6	–	NA	NA	NA
Sr	224.86	435	367	255	208.69	153	71	169	379.26	213	435	52	50	160	454	–	NA	NA	NA
Y	13.26	9	20.05	24	30.79	24	28	14	13.74	6	7	61	44	16	7.5	–	9.16	9.16	9.58
Zr	178.77	148	351.32	116	309.48	119	121	125	427.13	213	132	349	251	260	152	–	NA	NA	NA
Nb	8.96	10	9.81	11	27.42	26	21	15	9.87	7	9	28	34	18	6.4	–	NA	NA	NA
Ba	1122	1400	946.89	650	75.09	469	447	857	546.97	117	661	1215	239	920	690	–	NA	NA	NA
V	7.4	nd	15.89	nd	5.9	15	nd	nd	7.82	nd	nd	26	9	24		–	NA	NA	NA
La	12.52	nd	28.28	nd	23.46	nd	nd	nd	54.55	nd	nd	nd	nd	nd	32	76.67	67	85	78
Ce	27.50	nd	58.55	nd	51.49	nd	nd	nd	107.52	nd	nd	nd	nd	nd	56	118	104	133	117
Pr	3.55	nd	7.00	nd	6.44	nd	nd	nd	12.63	nd	nd	nd	nd	nd	nd	11.6	10	13	11.9
Nd	11.27	nd	21.15	nd	19.89	nd	nd	nd	37.80	nd	nd	nd	nd	nd	21.4	41.67	35	48	42
Sm	2.58	nd	3.79	nd	4.39	nd	nd	nd	6.38	nd	nd	nd	nd	nd	3.3	7.52	6.12	8.64	7.8
Eu	1.08	nd	1.00	nd	0.35	nd	nd	nd	0.80	nd	nd	nd	nd	nd	0.92	1.18	1.16	1.23	1.15
Gd	1.82	nd	2.90	nd	3.60	nd	nd	nd	4.93	nd	nd	nd	nd	nd	2.2	7.7	13.8	4.8	4.5
Tb	0.34	nd	0.50	nd	0.72	nd	nd	nd	0.69	nd	nd	nd	nd	nd	0.31	0.47	0.41	0.52	0.48
Dy	1.82	nd	2.55	nd	3.53	nd	nd	nd	2.61	nd	nd	nd	nd	nd	1.16	2.01	1.83	2.01	2.2
Ho	0.33	nd	0.47	nd	0.65	nd	nd	nd	0.36	nd	nd	nd	nd	nd	nd	0.39	0.34	0.39	0.45
Er	1.04	nd	1.52	nd	2.07	nd	nd	nd	1.0	nd	nd	nd	nd	nd	0.59	0.94	0.98	0.89	0.94
Tm	0.17	nd	0.26	nd	0.35	nd	nd	nd	0.12	nd	nd	nd	nd	nd	nd	0.12	0.11	0.12	0.12
Yb	1.14	nd	1.81	nd	2.42	nd	nd	nd	0.76	nd	nd	nd	nd	nd	0.55	0.66	0.74	0.64	0.62
Lu	0.2	nd	0.31	nd	0.41	nd	nd	nd	0.12	nd	nd	nd	nd	nd	0.12	0.09	0.12	0.08	0.08

* Trace element concentrations were determined by ICP-MS at NGRI, Hyderabad;

** Average of six gneisses occurring as enclave from G. Sarkar et al.(1993); +Average of 355 TTG from Martin (1994). Total iron as Fe_2O_3; LOI loss on ignition, nd not determined, Mg# = 100*Mg/(Mg+Fe)

*** Data after Sarkar et al. (1993), NA not analysed

Table 2 Representative major (wt%) and trace (ppm) element analyses of Bastar granitoids.

Sample No.	RB1	RB9	RB11*	RB20*	DK21*	Dk23	DK27	JT31	GD45	BP57	BS77	BSP98	BSP101*
SiO_2	70.92	72.45	75.6	72.75	65.6	73.46	71.35	71.25	72.13	74.6	66.7	68.7	70.6
TiO_2	0.25	0.17	0.08	0.23	0.4	0.11	0.25	0.36	0.11	0.36	0.53	0.41	0.13
Al_2O_3	14.13	13.97	12.5	12.94	12.5	13.37	13.83	15.3	14.8	14.4	16	15.64	15.9
$Fe_2O_3^t$	2.42	1.82	1.58	2.48	4.2	1.78	2.39	2.55	1.56	1.86	4.23	3.46	1.7
MgO	0.05	0.34	0.31	0.49	1.4	0.38	0.52	0.55	0.25	0.58	1.1	0.98	0.22
CaO	1.67	1.47	0.65	3.6	6	0.72	1.37	0.84	1	0.75	2.9	2.8	2.2
Na_2O	3.73	4.18	3.21	4.17	3	3.67	3.52	2.28	4.17	3.2	3.9	4.24	3.8
K_2O	4.56	4.01	5.43	1.95	4	4.98	4.76	3.38	5.12	3.41	4.5	2.79	6.8
MnO	0.03	0.02	0.01	0.03	0.14	0.03	0.03	0.02	0.02	0.02	0.05	0.04	0.02
P_2O_5	0.06	0.05	0.01	0.07	0.38	0.03	0.08	0.01	0.03	0.07	0.18	0.11	0.01
LOI	1.39	1.02	0.37	1.06	1.53	1.32	1.09	1.97	0.08	0.34	0.07	0.53	0.03
Total	**99.21**	**99.5**	**99.75**	**99.77**	**99.15**	**99.85**	**99.19**	**98.51**	**99.27**	**99.59**	**100.16**	**99.7**	**101.41**
Mg #	4	30	28	29	32	30	31	24	42	35	38	22	41
Cu	13.3	16.1	3.6	1.9	10.5	16.9	13.1	13.5	22.5	6	11	8	2
Ni	11.9	10.2	15.54	10	54	17.5	14.6	43.5	9.2	21	17.8	15.7	6
Co	nd	nd	69.03	3	56.5	nd	nd	nd	nd	nd	nd	nd	1.6
Sc	1.6	0.8	17.87	5	7.2	2.2	2.6	3.9	2.2	5	10.9	9.3	11.3
Zn	27.8	25.1	34	37	83.4	23.2	30.9	46.2	31	20	39.9	47	26.1
Ga	17.1	19.4	17	16	16.1	18.5	18.8	20.4	21	16	17.9	17.6	17.5
Pb	25	45	112	16	25.4	38	38	34	65	41	17	21	58.5
Cr	251	295	9.3	350	45.1	352	258	600	280	378	272	406	195
Th	21.9	10.5	72	16	15.7	60.3	41.5	43.2	33.4	34	8.1	8.9	86.4
Rb	136	124	348	44	116.7	284	182	183	187	116	73	90	263
U	3.7	6.2	22	1.5	3	12.9	7.7	7.8	7.3	4	1.8	1.3	8
Sr	283	269	47	410	812.8	86	159	239	176	127	386	358	271.2
Y	12	6	94	23	35.3	30	15	30	6	30	27	15	63.5
Zr	191	158	497	313	337	124	230	383	146	141	373	186	477
Nb	10	6	23	8	33	23	19	18	9	16	18	9	18.2
Ba	1495	1216	79	732	570	259	693	1009	842	469	1881	1119	399
V	nd	nd	2.45	17.6	nd	nd	nd	nd	nd	15	49	43	23
La	nd	nd	47.79	52.52	63.19	nd	nd	nd	nd	nd	nd	nd	64
Ce	nd	nd	110.06	109.21	171.9	nd	nd	nd	nd	nd	nd	nd	144.59
Pr	nd	nd	13.82	13.29	26.01	nd	nd	nd	nd	nd	nd	nd	18
Nd	nd	nd	41.69	40.22	88.13	nd	nd	nd	nd	nd	nd	nd	53.78
Sm	nd	nd	8.54	6.19	12.61	nd	nd	nd	nd	nd	nd	nd	9.6
Eu	nd	nd	0.206	1.22	2.2	nd		nd	nd	nd	nd	nd	0.55
Gd	nd	nd	7.07	4.48	8.94	nd	nd	nd	nd	nd	nd	nd	7.82
Tb	nd	nd	1.59	0.72	1.28	nd	nd	nd	nd	nd	nd	nd	1.56
Dy	nd	nd	9.07	3.21	5.31	nd	nd	nd	nd	nd	nd	nd	8.27
Ho	nd	nd	1.8	0.58	0.89	nd	nd	nd	nd	nd	nd	nd	1.56
Er	nd	nd	6.27	1.86	2.91	nd	nd	nd	nd	nd	nd	nd	4.75
Tm	nd	nd	1.09	0.28	0.42	nd	nd	nd	nd	nd	nd	nd	0.76
Yb	nd	nd	7.53	1.9	2.93	nd	nd	nd	nd	nd	nd	nd	4.97
Lu	nd	nd	1.22	0.3	0.48	nd	nd	nd	nd	nd	nd	nd	0.75

* Trace element concentrations were determined by ICP-MS at NGRI, Hyderabad;
Total iron as Fe_2O_3; LOI loss on ignition, nd not determined, Mg# = 100*Mg/(Mg+Fe)

K-Na-Ca diagram (Fig. 2), the gneisses plot along the calc-alkaline differentiation trend. The gneisses that occur as enclave (Sarkar G. et al., 1993) also plot along the calc-alkaline trend (Fig. 2). The multi-elemental patterns exhibited by the gneisses are fractionated with enriched LILE and depleted HFSE and with strong negative anomalies at P and Ti (Fig. 3). The chondrite normalized REE patterns (Fig. 4) are moderately to highly fractionated (La_N/Yb_N = 8-51). The patterns also exhibit HREE depletion and a concave curvature at the HREE ends.

3.2.2 Granitoids

The SiO_2 values of the granitoids ranges 65.5wt% to 75.6 wt%. The Al_2O_3 content of the granitoids (12.45 ≤ Al_2O_3 ≤ 16.01wt%) averages 14.25wt%, but for most of the rock samples the Al_2O_3 content is ≤ 15wt%. Like gneisses, the granitoids also show peraluminous nature, with the molar A/CNK values ranging from 1.16 to 1.35. The granitoids have relatively higher ferromagnesian content (Fe_2O_3+MgO+TiO_2 ranges from 2 to 6) and accordingly have relatively higher Mg # averaging 32 compared to the gneisses with average value of 29. The K/Rb values of the granitoids ranges from 130 - 368, which are broadly comparable to the commonly occurring calc-alkaline suites (Bertrand et al., 1984). Only one sample (BS77), with low Rb content (73ppm) shows exceptionally high K/Rb value (508). The values for Zr/Hf (26-52), Rb/Sr (<1), Rb/Zr (0.2-2.3) and Nb/Ta (1-13) of the granitoids are in the range of plutonic rocks found in continental magmatic arc (Ayuso and Arth, 1992). Almost all the granitoids have high K_2O values compared to the Na_2O values and the ratio K_2O/Na_2O averages 1.2. Like the gneisses, the granitoids also plot along the calc-alkaline differentiation trend on the K-Na-Ca diagram (Fig. 2). The multi-elemental patterns of the granitoids exhibit that LILE (especially Rb, Ba, Th, U and K) are enriched in comparison to the HFSE (Fig.3). Among the HFSE, Ti and P are strongly depleted and Nb relatively weakly depleted with respect to the neighbouring elements (Fig. 3). The REE patterns of the granitoids are flat at light REE and heavy REE with depletion at middle REE with strong to insignificant Eu anomalies (Fig. 4).

3.2.3 Mafic Dykes

The Bastar mafic dykes in general have low SiO_2 (48-

Table 3 Representative major (wt%) and trace (ppm) element analyses of mafic dykes of Bastar craton.

	Amphibolite						Dolerite				
Sample No	RB12	GD32	GD34	GD37	GD43	BP58	RB4	RB16	GD40	GK52	BP63
SiO_2	49.89	51.25	49.31	51.2	49.86	49.18	56.58	50.64	48.04	49.56	51.01
TiO_2	1.23	0.37	1.06	1.3	0.86	0.99	0.9	1.65	2.49	2.31	0.59
Al_2O_3	13.29	7.33	11.89	12.59	12.56	12.71	14.7	11.76	11.74	13.42	9.04
Fe_2O_3*	14.93	16.17	14.16	14.83	13.75	15.11	8.49	15.74	17.14	18.21	14.11
MgO	7.61	6.68	7.52	5.6	7.49	8.28	5.15	6.08	6.29	4.87	14.6
CaO	10.72	10.78	10.82	9.94	10.78	11.16	6.18	7.54	8.48	8.89	8.34
Na_2O	1.96	0.34	2.23	2.14	1.7	1.97	3.49	1.46	2.06	2.06	1.4
K_2O	0.31	1.78	0.43	0.62	0.58	0.24	2.29	2.5	1.13	0.98	0.68
MnO	0.19	4.08	0.2	0.2	0.19	0.19	0.11	0.32	0.24	0.23	0.19
P_2O_5	0.12	0.14	0.16	0.27	0.19	0.07	0.53	0.41	0.44	0.2	0.06
LOI	nd	1.02	1.93	1.26	1.98	nd	1.17	1.38	1.03		
Total	100.25	99.94	99.71	99.95	99.94	99.9	99.59	99.48	99.08	100.73	99.98
Mg#	50	45	46	42	52	52	55	44	42	35	67
Cu	178.4	37.7	162.7	155.93	159.8	221.7	35.2	33.5	245.81	274.93	89.2
Ni	114.2	96.4	114.7	61	133.2	124	45.3	82.2	88.42	58.58	416.5
Co	nd	34	43	64.7	51	nd	26	52	68.16	58.36	nd
Sc	47	15	42	35.13	43	48	16	38	50.83	46.38	36
V	329	nd	nd	298.45	nd	368	nd	nd	256.19	348.12	203
Zn	103.7	109	98.3	101.24	97.1	93.1	81.5	184.5	135.52	149.24	77.2
Ga	16.6	14.7	18.2	18.16	16	13.7	19.7	24.4	18.49	20.11	9.8
Pb	6	7.7	1.1	5.58	1.8	3	1.4	10.5	5.24	6.03	6
Cr	340	435	374	69.3	277	312	317	270	134.83	142.93	1789
Th	0.8	6.7	1.5	1.63	1.4	1	14.9	3.1	3.2	2.81	0.5
Rb	13	49.1	24.3	27.25	23.9	10	122.1	117.5	32.38	46.64	27
U	0.4	0.9	0.3	1.31	0.3	0.4	3.4	2.6	1.48	2.39	1.1
Sr	153	17	132	164.99	129	118	531	117	126.53	183.49	173
Ba	23	1004	51	230.61	96	17	1011	153	307.22	234.31	131
Nb	4	13.8	4.4	9.44	4	4	16.8	19.3	16.28	14.69	4
Zr	84	102	59	53.32	72	61	243	160	205.73	189.4	86
Y	24	23.2	22	32.85	24.1	21	27.7	51.5	48.73	46.21	15
La	nd	9.45	nd	4.96	nd	nd	nd	nd	10.84	10.07	nd
Ce	nd	32.59	nd	20.3	nd	nd	nd	nd	41.62	38.47	nd
Pr	nd	3.8	nd	2.81	nd	nd	nd	nd	5.81	5.3	nd
Nd	nd	13.66	nd	11.8	nd	nd	nd	nd	23.99	21.91	nd
Sm	nd	3.28	nd	3.29	nd	nd	nd	nd	6.25	5.65	nd
Hf	nd	1.47	nd	1.66	nd	nd	nd	nd	4.83	4.42	nd
Eu	nd	1.07	nd	1.12	nd	nd	nd	nd	1.63	1.78	nd
Gd	nd	3.21	nd	3.84	nd	nd	nd	nd	6.98	6.4	nd
Tb	nd	0.52	nd	0.73	nd	nd	nd	nd	1.23	1.13	nd
Dy	nd	3.18	nd	4.89	nd	nd	nd	nd	7.78	7.1	nd
Ho	nd	0.56	nd	0.88	nd	nd	nd	nd	1.35	1.27	nd
Er	nd	1.79	nd	2.98	nd	nd	nd	nd	4.4	4.11	nd
Tm	nd	0.28	nd	0.47	nd	nd	nd	nd	0.69	0.63	nd
Yb	nd	1.76	nd	2.91	nd	nd	nd	nd	4.21	3.87	nd
Lu	nd	0.28	nd	0.46	nd	nd	nd	nd	0.66	0.61	nd

Major elements in wt%; Trace elements in ppm; Total Iron as Fe_2O_3*; L.O.I. Loss on Ignition;
nd, not determined; Mg# = 100xMg/(Mg+Fe) assuming FeO/FeO* = 0.85.

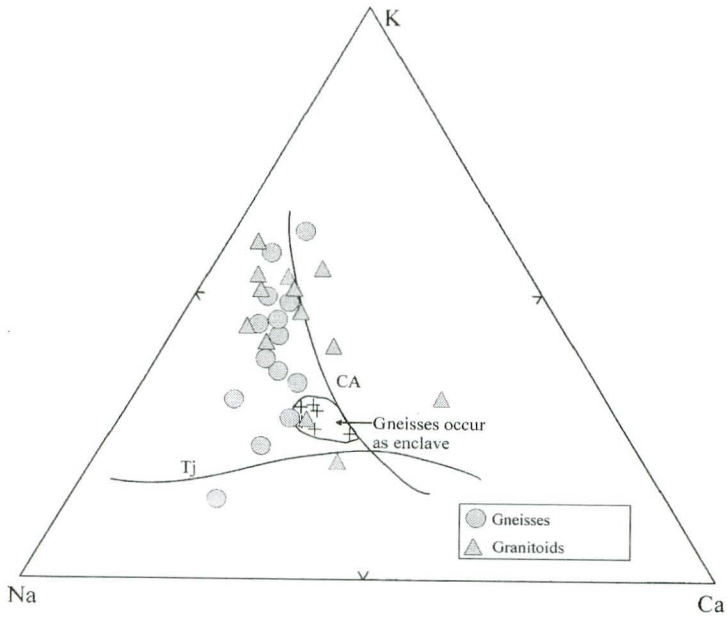

Fig. 2 K-Na-Ca diagram of gneisses and granitoids of Bastar craton. For comparison, gneisses occurring as enclaves are also shown (data after Sarkar, G. et al., 1993). Calc-alkaline (CA) and trondhjemite (Tj) trends are after Barker and Arth (1976).

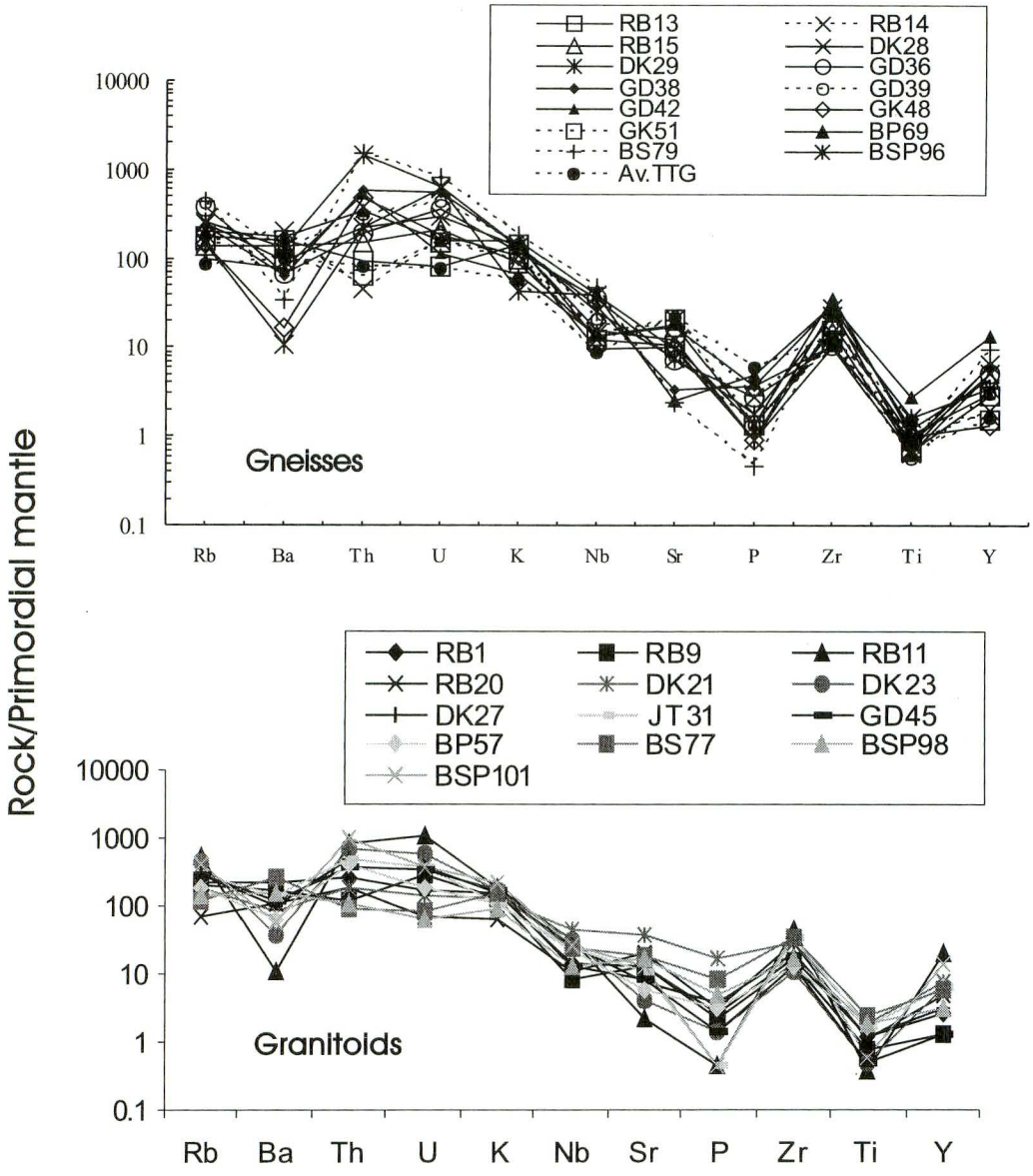

Fig. 3 Primordial mantle normalized multi-element patterns for the gneisses and granitoids of Bastar craton. For comparison, an average of 355 Archaean TTG (values from Martin, 1994) are plotted with the gneisses. Normalizing values are from Sun and McDonough (1989).

51 wt%), low MgO (4-7 wt%) and TiO_2 (<2.5 wt%) contents with Mg# clustering between 42 and 55. On AFM plot (Irvine and Baragar, 1971), the dykes exhibit tholeiite trend and group them as iron rich tholeiites (Fig. 5). One sample BP-63 is the most primitive with Mg# equals 67 and MgO equals 15 wt%; while sample GK-52 is the most evolved with Mg# equals 35 and MgO equals 4.87 wt% among the studied Bastar mafic dykes. The multi-element patterns of the amphibolite group of dykes show nearly flat, less fractionated patterns with low LILE/HFSE ratios (Fig. 6) and the dolerites exhibit a moderately fractionated pattern with distinct Sr, P and Ti anomalies (Fig. 6). Both CaO and Al_2O_3 for the dolerites show a decreasing trend with increasing Mg #, but for the amphibolites a well-defined positive relationship is observed between CaO and Mg # (Fig. 7). CaO/Al_2O_3 of both the amphibolite and dolerites is always lower than that of the value of chondrite (0.9). These features account for clinopyroxene fractionation for the amphibolite dykes in particular. Ni and Cr show positive relationship with Mg#. The most primitive sample (BP-63) does contain Cr ~1800ppm and Ni ~420ppm which reflect ferromagnesian phenocrystic nature of the sample. In other samples, the concentrations of these elements Ni (45-135 ppm) and Cr

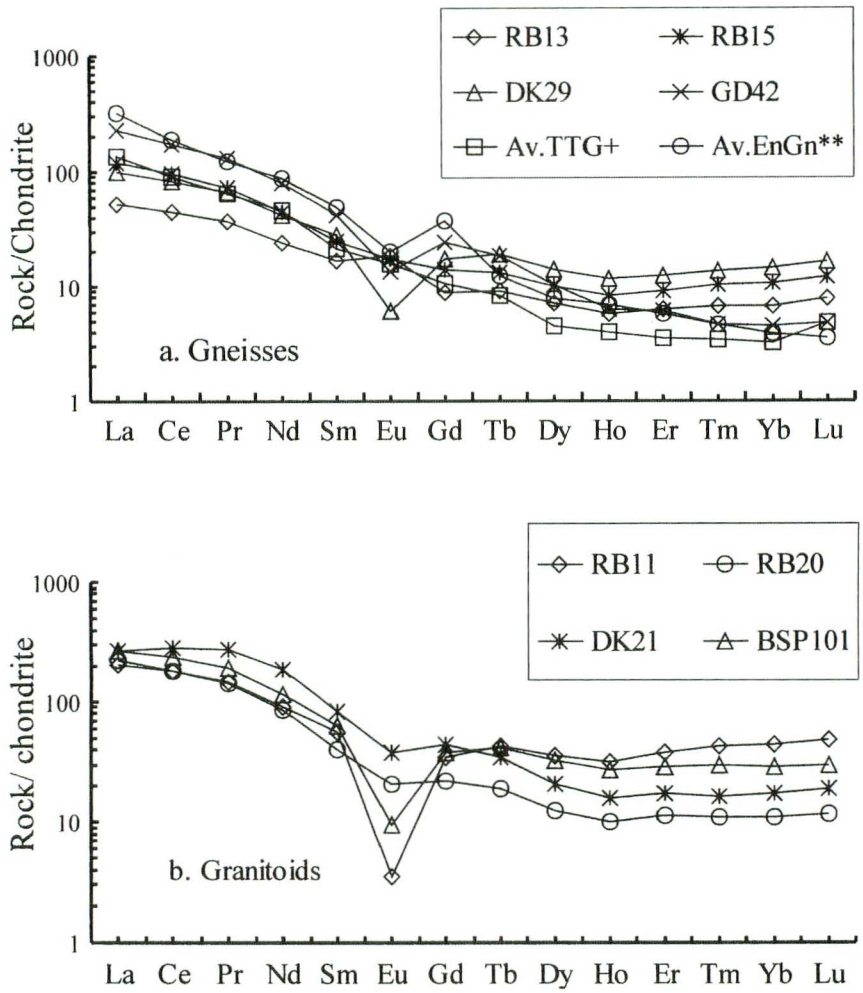

Fig. 4 Chondrite normalized rare earth element patterns for the gneisses and granitoids of Bastar craton. For comparison, gneisses that are occurring as enclaves (Av. EnGn**) within the craton (values from Sarkar, G. et al., 1993) and an average of 355 Archaean TTG (Av TTG+) of Martin (1994) are plotted with the gneisses of Bastar craton. Normalizing values are from Sun and McDonough (1989).

(190-440ppm) confirm fractional crystallization involving ferromagnesian minerals (olivine + pyroxene) as suggested based on CaO-Mg # relationship. The Bastar mafic dykes show a good positive correlation between Zr/Y and Zr (Fig. 8) indicating fractionation of clinopyroxene and amphibole (Floyd, 1993). Two calculated partial melting curves (Drury, 1983) corresponding to two sets of source mineralogy (curve I: olivine 60%+orthopyroxene 20%+clinopyroxene 10%+ plagioclase 10%; curve II: olivine 60%+orthopyroxene 20%+clinopyroxene 10%+ garnet 10%) for Archaean mantle source (Sun and Nesbitt, 1977) were drawn in the diagram. Most of the dolerite samples plot along curve I indicating olivine, orthopyroxene, clinopyroxene and plagioclase as the dominant mineralogy of the source, whereas the amphibolite samples plot between the two curves indicating their generation from a different source consisting of olivine, orthopyroxene, clinopyroxene and garnet. The chondrite normalized rare earth element (REE) patterns (Fig. 9) of the dykes of Bastar craton exhibit enriched abundances of these elements relative to chondrite by more than 10 times over the entire range of rare earth elements (REE). Within the groups, the dolerites exhibit relatively higher level of enrichment of the entire REE spectrum than do the amphibolites. The dolerites are also characterized by a small negative anomaly at Eu indicating plagioclase fractionation (Fig. 9).

4. Petrogenesis and Tectonic Setting

4.1 Gneisses and granitoids

The primordial mantle normalized multi-elemental

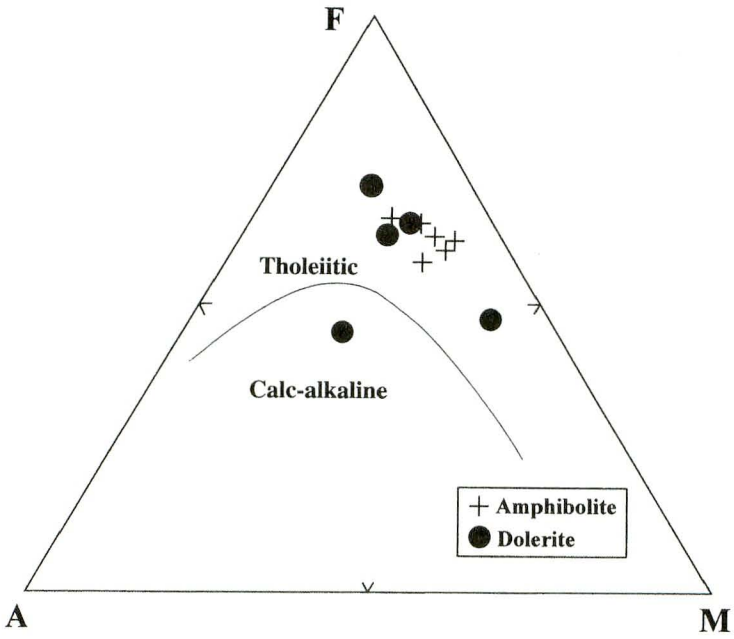

Fig. 5 AFM diagram for the mafic dykes of Bastar craton. Fields after Irvine and Baragar (1971).

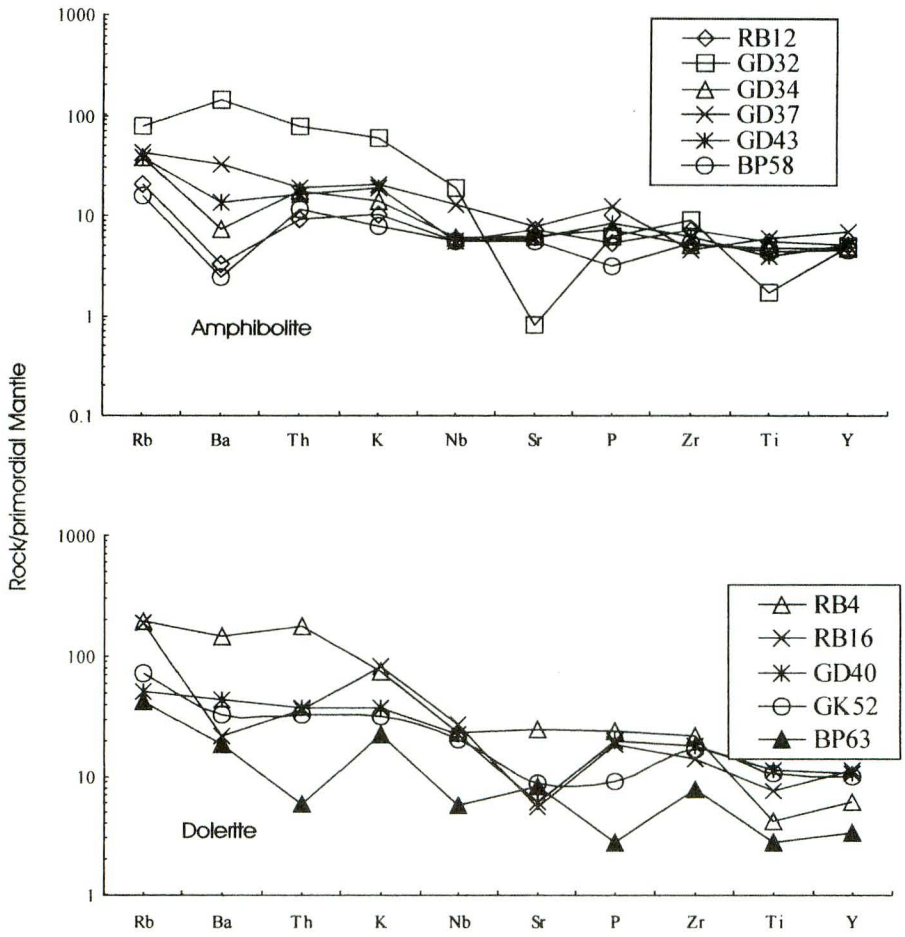

Fig. 6 Primordial mantle normalized multi-element pattern for amphibolite and dolerite group of dykes of Bastar craton. Normalizing values are from Sun and McDonough (1989).

patterns (Fig. 3) for both the gneisses and granitoids show marked enrichment in the LILE with enriched abundances in Rb, Th, and U. The patterns simultaneously display lesser abundances of HFSE with strong negative anomalies at P and Ti. Such incompatible elemental patterns displayed in the spidergram (Fig. 3) may be explained by magmatism in a subduction zone environment (Peacock, 1990; Saunder et al., 1991; Hawkesworth et al., 1994). To understand the degrees and trends of partial melting and to constrain the source characteristics, the gneisses and granitoids are plotted on the Sr/Y vs. Y diagram (Fig. 10). Four melting curves modeled presuming different sources like an average MORB and an Archaean mafic composite computed from Archaean basaltic and komatitic basalt following Drummond and Defant (1990) are superimposed on the diagram. Most of the samples plot along the partial melting Curve-II corresponding to partial melting of an average MORB leaving a 10% garnet amphibolite restite (Fig. 10). It is proposed that an Archaean oceanic slab while subducting, might have undergone higher degrees of

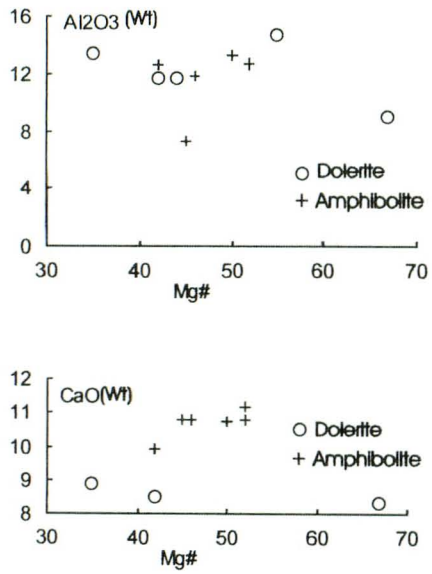

Fig. 7 Mg# vs. CaO and Al_2O_3 plot of the mafic dykes of Bastar craton.

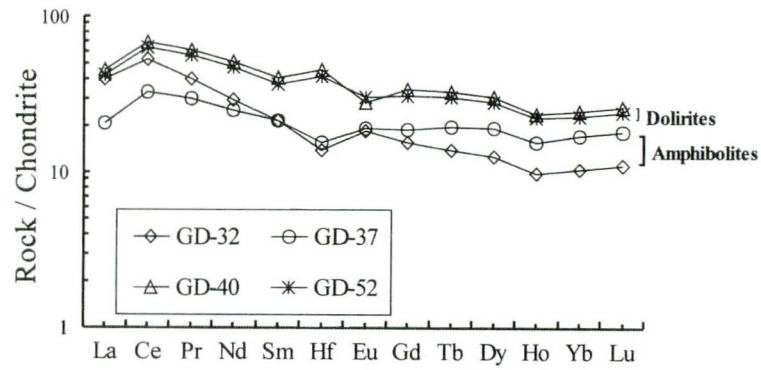

Fig. 9 Chondrite normalized REE patterns of representative samples of dolerite and amphibolite group of dykes of Bastar craton. Normalizing values are from Sun and McDonough (1989).

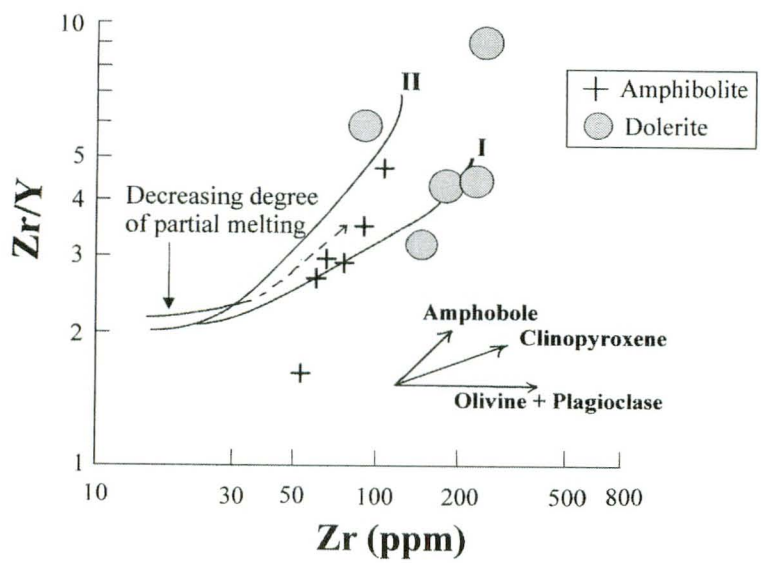

Fig. 8 Binary plot of Zr/Y vs. Zr for the mafic dykes of Bastar craton. Melting curves (I and II) are after Drury (1983) and vectors for fractional crystallization are after Floyd (1993).

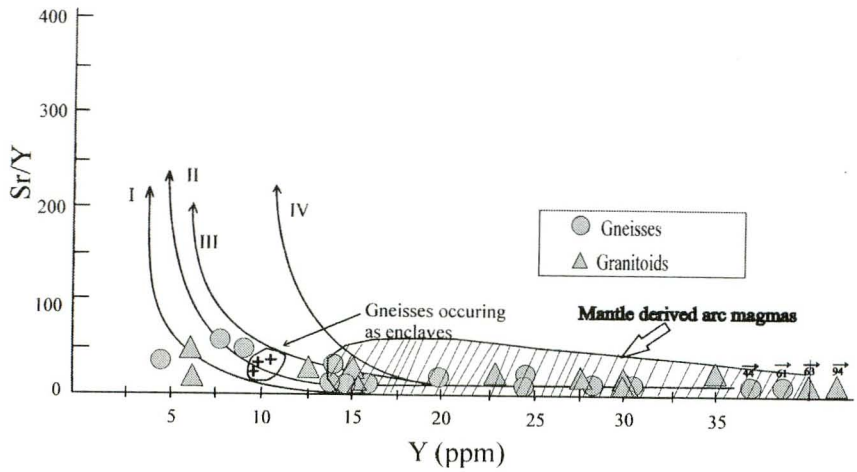

Fig. 10 Y vs. Sr/Y diagram for the Bastar gneisses and granitoids. For comparison, gneisses occurring as enclaves are shown (values from Sarkar, G. et al., 1993). Curves are after Drummond and Defant (1990). I and III are partial melting curves of an average Mid-Oceanic Ridge Basalt (MORB) and an Archaean Mafic Composite (AMC) leaving an eclogite restite. II and IV are partial melting curves of MORB and the AMC leaving a 10% garnet amphibolite restite.

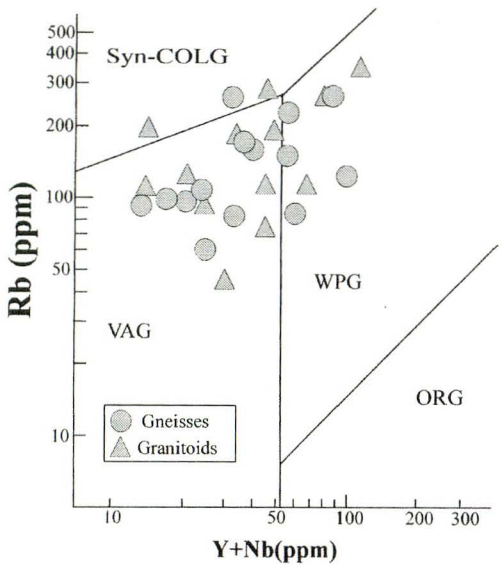

Fig. 11 Rb vs. Y+Nb tectonic variation diagram for the gneisses and granitoids of Bastar craton. Fields: VAG volcanic arc granite, Syn-COLG syn-collision granite, WPG within plate granite, ORG ocean ridge granite (after Pearce et al., 1984).

partial melting to generate the precursor melts for the Bastar gneisses. Similar mechanism can also be proposed for the generation of the granitic melt at a later stage during Proterozoic. The REE patterns (Fig. 4) are moderately to highly fractionated for the gneisses (La_N/Yb_N = 8-51). The patterns also exhibit HREE depletion and concave shape with curvature of the HREE position (Fig. 4). This is typical of Archaean silicic gneisses (Martin, 1986, 1994) and is generally considered to indicate the involvement of hornblende and/or garnet in this genesis (Tarney et al., 1979, Compton, 1978, Weaver and Tarney, 1981, Martin 1993). Both positive and negative Eu anomalies are observed in the Bastar gneisses (Fig. 4), while the Eu anomalies are insignificant in the Archaean TTG (Martin, 1994). The gneisses are characterized by slightly higher Yb_N values (average 9) than that of typical Archaean TTG value (<5); high La_N/Yb_N ratios ranging from 5.7 - 39.3; HREE depletion patterns with positive and negative Eu anomalies. To account for these features, it can be proposed that both fractional crystallization of hornblende (for positive Eu anomaly) and plagioclase (for negative Eu anomaly) and partial melting of an Archaean mafic source (amphibolite/eclogite (?)] with garnet and/or hornblende in the residuum. The REE patterns of the granitoids (Fig. 4) exhibit fractionated trends (La_N/Yb_N = 5-20) with strong to insignificant negative Eu anomaly. The sample with least slope (La_N/Yb_N = 5) has the strongest negative Eu anomaly and the sample with maximum slope (La_N/Yb_N=19) has an insignificant Eu anomaly. The convergent plate margin magmatic setting for the gneisses and granitoids of the Bastar craton is also established in the Rb vs. (Y+Nb) diagram (Fig. 11) of Pearce et al., (1984). Most of the samples plot within the volcanic arc granite (VAG) field; a few samples of gneisses and granitoids plotting on the within plate granite (WPG) field (Fig. 11). This indicates that the granitoids and the protoliths of the gneisses were emplaced in an arc related magmatic setting. The time spans between the ages of emplacement of the protoliths of gneisses (3.5Ga) and the youngest granitoids emplaced (1.5Ga), is of about 2000 Ma. Thus a single and

uninterrupted subduction event may not account for the genesis of the protoliths of the gneisses and the granitic magma. However two distinct phases of subduction, one in Archaean and the other during Proterozoic were probable for the genesis of the gneisses and the granitoids. Moreover the tectonic mode of subduction might have varied from Archaean to Proterozoic. The gneisses having low Mg # (29), Ni (12ppm), Cr (273ppm), Ba (690ppm), Sr (225ppm) and P_2O_5 (0.08ppm) content thus reflects that the melts released from the subducting slab had lesser interaction with the mantle wedge. A flat low angle subduction (under-thrusting of the oceanic crust) model of Smithies and Champion (2000), wherein the melts from the subducting slab ascends without much interaction with the mantle wedge, seems the probable tectonic mode of subduction for the Bastar Archaean gneisses. But for the granitoids, with geochemical features typical of convergent margin magmatic setting (Fig. 11) are additionally characterized by average high Mg # (33), Ni (19ppm), Cr (284ppm), Sr (280ppm), Ba (830ppm), P_2O_5 (0.08wt%) and Zr (275ppm). Such progressive increase in the elemental abundances in the granitoids can be explained in terms of melt - mantle wedge interaction.

4.2 Mafic dykes

On the primordial mantle normalized multi-element diagram (Fig. 6) the amphibolite dykes exhibit elevated LILE than HFSE, flat HFSE pattern and a low LILE/HFSE ratio which can be explained by higher degrees of partial melting from a trace element enriched region in the mantle that is likely to be modified by intraplate (within plate) enrichment processes induced by mantle plumes. In contrast, the dolerites are characterized by both LILE and HFSE enrichment than primordial mantle, high LILE/HFSE ratios and moderately fractionated trends with strong negative Nb, P and Ti anomalies (Fig. 6). This trend can be explained by a low degree of partial melting of an enriched mantle region in the asthenospheric mantle which can likely be modified by subduction related processes followed by fractionation of plagioclase and titano-magnetite during ingress of magma through crustal layers en-route to the surface. The REE patterns of the dolerites exhibit relatively higher level of enrichment of the entire REE spectrum than do the amphibolites (Fig. 9). The multi elemental patterns (Fig. 6) and the REE patterns (Fig. 9) of the Bastar mafic dykes thus indicate that the melts for both the groups of dykes might have been inherited from different mantle sources by different degrees of melting. Srivastava et al. (1996) have suggested that the amphibolite dykes were derived from an earlier relatively high Mg, low Ti olivine tholeiitic magma, while the dolerite dykes were derived from a low Mg, high Ti quartz tholeiitic magma.

The observed higher values of Rb/Ba in the Ti/Y vs. Rb/Ba ratio-ratio plot (Fig. 12) of the Bastar mafic dykes thus indicate either the influence of crustal material or an inherited mantle characteristic. In the Ti/Y vs. Rb/Ba diagram, Bastar mafic dykes samples plot around low Ti CFB field of Hergt et al. (1991) in terms of Ti/Y ratios but

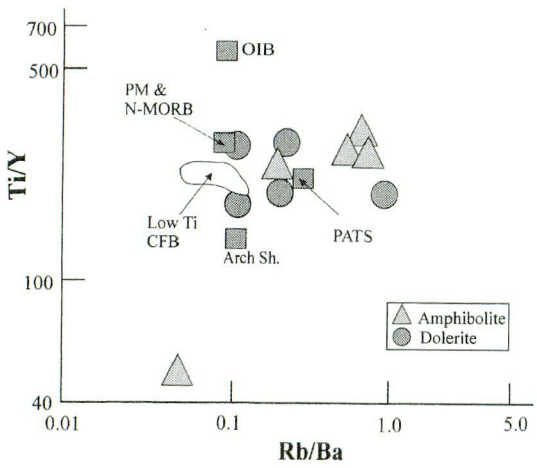

Fig. 12 Ti/Y vs. Rb/Ba plots for the Bastar mafic dykes. Values for N-MORB(N-type Mid Oceanic Ridge Basalt), OIB (Ocean Island Basalt) and PM (Primordial Mantle) after Sun and McDonough (1989); Archaean shale (Arch Sh) after McLennan et al. (1983) and post Archaean Terrestrial shale (PATS) after Taylor and McLennan (1985). Low-Ti CFB field after Hergt et al. (1991).

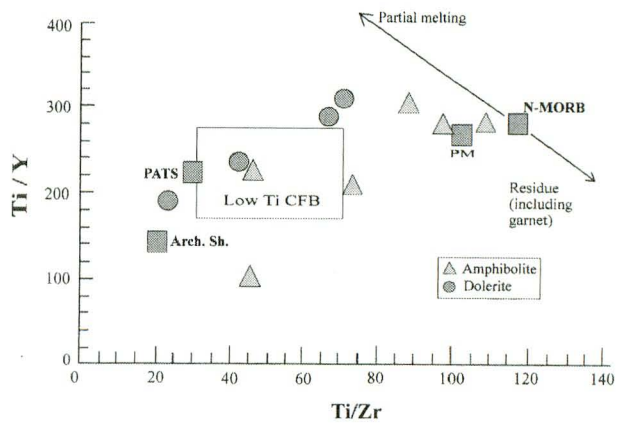

Fig. 13 Ti/Y vs. Ti/Zr plot for the Bastar mafic dykes. Values for N-MORB and PM after Sun and McDonough (1989); Archaean shale (Arch Sh) after McLennan et al. (1983) and post Archaean Terrestrial shale (PATS) after Taylor and McLennan (1985). Low-Ti CFB field after Hergt et al. (1991).

these samples invariably have higher Rb/Ba values with respect to PATS (Fig. 12). One sample GD-32 shows very low Ti/Y value because of extremely low TiO_2 (TiO_2 = 0.37 wt%) content. One of the possibilities for the observed crustal signature of these dykes may be due to introduction of sediments into the mantle. Both the amphibolite and dolerite group of dykes of the Bastar craton do show a good positive correlation in the Ti/Y vs. Ti/Zr diagram (Fig. 13). The dolerites have comparatively lower Ti/Y and Ti/Zr values plotting around the low Ti continental flood basalt (CFB) fields of Hergt et al. (1991); while some of the amphibolite dykes with high Ti/Y and Ti/Zr plot closer to N-MORB and PM values in the Ti/Y vs. Ti/Zr diagrams (Fig. 13). Hergt et al. (1991) have pointed out that on melting, the residual source (s) would yield abnormally low Ti/Y values while the derived magmas would have higher Ti/Zr values. The low Ti/Y and Ti/Zr values for the dolerite dykes of Bastar craton and its plot around low Ti CFB field of Hergt et al. (1991) (Fig. 13) thus indicate sediment incorporation into the mantle as one of the possible mechanisms. In contrast, the higher Ti/Y and Ti/Zr values and their plot around N-MORB and PM for the amphibolite dykes (Fig. 13) of Bastar craton thus indicate somewhat different mantle enrichment processes.

5. Conclusion

Geochemical features of the Bastar gneisses are broadly comparable to the rocks commonly occurring along convergent margin tectonic setting (Bertrand et al., 1984) and thus invoke a subduction mechanism for the petrogenesis of the precursor melts of the gneisses. The second episode of magmatism during Proterozoic is represented by bimodal magmatism consisting of granitoids and mafic dykes. The granitoids bear compositional similarities with the gneisses. Major element features for the granitoids along with inter-elemental ratios like K/Rb (130-368), Zr/Hf (26-52), Rb/Sr (<1), Rb/Zr (0.2-2.3), Nb/Ta (1-13) indicate an arc related magmatic setting for the granitoids as well. Two distinct phases of subduction, one in the Archaean for the gneisses and the other in the Proterozoic for the granitoids seem probable for the genesis of the granitoids and the protoliths of the gneisses. Moreover the tectonic mode of subduction might have varied from Archaean to Proterozoic. The gneisses having low Mg #, Ni, Cr, Ba, P_2O_5 and Sr content reflect that the magma generated by partial melting of the subducting slab might have risen without much interaction with the mantle wedge. A flat low angle subduction (under-thrusting of the oceanic crust) model of Smithies and Champion (2000), wherein the melts from the subducting slab ascends without encountering the mantle wedge, seems the probable tectonic mode of subduction for the Bastar Archaean gneisses. In contrast the granitoids having relatively high Mg#, high Ni, Cr, Sr, Ba and P_2O_5 contents reflect melt - mantle wedge interaction. Thus the petrogenesis of the granitoids invokes a modern type of subduction during the Proterozoic.

The REE patterns of the mafic dykes (Fig. 9), multi-elemental patterns (Fig. 6), Ti/Y, Ti/Zr, Rb/Ba values and the plots of the ratios on the Rb/Ba vs. Ti/Y (Fig. 12) and Ti/Y vs. Ti/Zr (Fig.13) indicate that the melts for both the groups of dykes might have been derived from different mantle sources. Since the genesis of the granitoids during Proterozoic invoked a modern type subduction, incorporation of sediments up to a shallower depth into the mantle via such subduction can account for the observed geochemical features of the dolerite dykes. In contrast the geochemical features presented earlier for the amphibolite dykes indicate a deeper mantle source region which might have developed through mantle metasomatic processes. Melting of these enriched deep mantle sources could be related to lithospheric extension/rifting during the Proterozoic period, as suggested for adjoining Bundelkhand area in the north (Mondal and Ahmad, 2001) and Aravalli craton in the northwest (Ahmad and Tarney, 1994). Thus our study suggests multiphase subduction and lithospheric extension/rifting for the growth of the Bastar continental nucleus. It is also proposed that the dominant magmatism during Archaean in the Bastar craton was felsic which changed to bimodal (acidic-basic) magmatism during Proterozoic.

Acknowledgements

The authors thank the Directors of WIHG, Dehra-Dun and NGRI, Hyderabad and the Chairman, Department of Geology, AMU, Aligarh and Chairman, Department of Geology, University of Delhi, New Delhi for providing facilities to carry out the study. MEAM thankfully acknowledges the financial assistance by DST, Govt. of India (HR/SY/A-08/97). We are grateful to Dr. K. Furuyama, Osaka City University and Dr. M. Satish-Kumar, Shizuoka University, Japan for constructive and helpful reviews that led to considerable improvements in the final version of the manuscript.

References

Ahmad, T. and Tarney, J. (1994) Geochemistry and petrogenesis of late Archaean Aravalli volcanics,

basement enclaves and granitoids, Rajasthan. *Precambrian Res.* **65**, 1-23.

Asthana, D., Desh, M.R., Pophare, A.M. and Khare, S.K. (1996) Interstratified low-Ti and High-Ti volcanics in arc-related Khairagarh Group of Central India. *Current Sci.* **71**, 304-306.

Ayuso, R.A. and Arth, J.G. (1992) The northeast kingdom batholith, Vermont: magmatic evolution and geochemical constraints on the origin of Acadian granitic rock. *Contrib. Mineral. Petrol.* **111**, 1-23.

Balaram, V., Ramesh, S.L. and Anjaiah, K.V. (1996) New trace and REE data in thirteen GSF reference samples by ICP-MS. *Geostandards Newsletter* **20**, 71-78.

Barker, F. and Arth, J.G. (1976) Generation of trondhjemite-tonalitic liquids and Archaean bimodal trondhjemites - basalt suits. *Geology* **4**, 596-600.

Bertrand, J.M., Dupuy, C., Dostal, J. and Davison, I. (1984) Geochemistry and geotectonic interpretation of granitoids from central Iforas (Mali, W. Africa). *Precam. Res.* **26**, 265-283.

Compton, P. (1978) Rare-earth evidence for the origin of the Nuk gneisses, Buksefjorden region, Southern West Greenland. *Contrib. Mineral. Petrol.* **66**, 283-294.

Crookshank, H. (1963) Geology of southern Bastar and Jeypore from Bailadila range to the Eastern Ghat. *Memoir Geol. Surv. India* **87**, pp. 149.

Drummond, M.S. and Defant, M.J. (1990) A model for trondhjemite-tonalite - dacite gneisses and crustal growth via slab melting: Archaean to modern comparisons. *J. Geophys. Res.* **95B**, 21503-21521.

Drury, S.A. (1983) The petrogenesis and tectonic setting of Archaean metavolcanics from Karnataka state, south India. *Geochim. Cosmochem Acta*, **47**, 317-329.

Floyd, P.A. (1993) Geochemical discrimination and petrogenesis of alkali basalt sequences in parts of Ankara melange, central Turkey. *J. Geol. Soc. London*, **105**, 541-550.

Hawkesworth, C.J., Gallagher, K. Hergt, J.M. and McDermott, F. (1994) Destructive plate margin magmatism: Geochemistry and melt generation. *Lithos*, **33**, 169-188.

Hergt, J.M., Peate, D.W. and Hawkesworth, C.J. (1991) The petrogenesis of Mesozoic Gondwana low-Ti flood basalts. *Earth Planet. Sci. Lett.* **105**, 134-148.

Hussain, M.F., Mondal, M.E.A. and Ahmad, T. (2004) Geochemistry of basement gneisses and gneissic enclaves from Bastar craton: geodynamic implications. *Current Sci.* **86**, 1543-1547.

Irvine, T.N. and Baragar, W.R.A. (1971) A guide to the chemical classification of the common rocks. *Canadian J. Earth Sci.*, **8**, 523-548.

Martin, H. (1986) Effect of Steeper Archaean geothermal gradient on geochemistry of subduction zone magmas. *Geology*. **14**, 753-756.

Martin, H. (1993) The mechanisms of petrogenesis of the Archaean continental crust, comparison with modern processes. *Lithos*, **30**, 373-388.

Martin, H. (1994) The Archaean grey gneisses and the genesis of continental crust. In: Condie, K. C. (Ed.), Archaean Crustal Evolution, Elsevier, Amsterdam, pp. 205-259.

McLennan, S.M., Taylor, S.R. and Erikson, K.A. (1983) Geochemistry of Archaean shales for the Pilbara Supergroup, western Australia. *Geochim. Cosmochim. Acta*, **47**, 1211-1227.

Mishra, V.P., Dutta, N.K., Kanchan, V.K., Vatsa, U.S. and Guha, K. (1984) Archaean granulite and granite gneiss complexes of Kondagaon area, Bastar district, M.P. *Record Geol. Surv. India*, **113**, part 6, pp. 150-158.

Mondal, M.E.A. and Ahmad, T. (2001) Bundelkhand mafic dykes, Central Indian Shield: implication for the role of sediment subduction in Proterozoic crustal evolution. *The Island Arc*, **10**, 51-67.

Neogi, S., Miura, H. and Hariya, Y. (1996) Geochemistry of the Dongargarh volcanic rocks, central India: implications for the Precambrian mantle. *Precambrian Res.*, **76**, 77-91.

Peacock, S.M. (1990) Numerical Simulation of metamorphic pressure - temperature - time paths and fluid production in subducting slabs. *Tectonics*, **9**, 1197-1211.

Pearce, J.A., Harris, N.B.W. and Tindle, A.G. (1984) Trace element discrimination diagrams for the tectonic interpretations of granitic rocks. *J. Petrol.* **25**, 956-983.

Radhakrishna B.P. and Naqvi, S.M. (1986) Precambrian continental crust of India and its evolution. *J. Geol.*, **94**, 145-166.

Ramakrishnan, M. (1990) Crustal development in Southern Bastar, Central Indian craton. *Geol. Surv. India Spec. Publ.* No.**28**, pp.44-66.

Saini, N.K., Mukherjee, P.K. Rathi M. S., Khanna P.P. and Purohit, K.K. (1998) A new geochemical reference sample of granite (DG-H) from Dalhousie, Himachal Himalaya. *J. Geol. Soc. India*, **52**, 603-606.

Sarkar, A., Sarkar,G., Paul, D.K. and Mitra N.D. (1990) Precambrian Geochronology of the Central Indian Shield - A Review. *Geol. Surv. India Spec. Publ.* No.**28**, pp. 453-482.

Sarkar, G., Corfu, F., Paul, D.K., McNaughton, N.J.,

Gupta, S.N. and Bishui, P.K. (1993) Early Archaean crust in Bastar craton, central India - a geochemical and isotopic study. *Precambrian Res.*, **62**, 127-137.

Sarkar, G., Gupta, S.N. and Bishui, P.K. (1994) New Rb-Sr isotope ages and geochemistry of granitic gneisses from southern Bastar: implications for crustal evolution. *Indian Minerals*, **48**, 7-12.

Saunder, A.D., Norry, M.J., Tarney, J. (1991) Fluid influence on the trace element composition of subduction zone magmas. *Phil. Trans. Royal Soc. London*, **335**, 377-392.

Smithies, R.H. and Champion, D.C. (2000) The Archaean high Mg diorite suite: Links to tonalite-trondhjemite-granodiorite magmatism and implications for early Archaean crustal growth. *J. Petrol.*, **41**, 1653-1671.

Srivastava, R.K., Hall, R.P., Verma, R. and Singh, R.K. (1996) Contrasting Precambrian mafic dykes of the Bastar craton, central India: petrological and geochemical characteristics. *J. Geol. Soc. India*, **48**, 537-546.

Sun, S.S. and Mc Donough, W.F. (1989) Chemical and isotopic systematics of oceanic basalts: implications for mantle compositions and Processes. In : Saunders, A.D., Norry, M.J. (Eds.), Magmatism in the Ocean Basins. *Geol. Soc. London Spec. Publ.*, **42**, 315-345.

Sun, S.S. and Nesbitt, R.W. (1977) Chemical heterogeneity of the Archaean mantle composition of the bulk earth and mantle evolution. *Earth Planet. Sci. Lett.*, **35**, 429-448.

Tarney, J., Weaver, B.L. and Drury, S.A. (1979) Geochemistry of Archaean trondhjemitic and tonalitic gneisses from Scotland and East Greenland, In: Barker, F. (Ed.), Trondhjemites, Dacites and Related Rocks, Elsevier, Amsterdam, pp. 275-299.

Taylor, S.R. and McLennan, S.M. (1985) The continental crust: its composition and evolution. Blackwell, Oxford.

Weaver, B.L. and Tarney, J. (1981) Lewisian gneiss chemistry and Archaean crustal development models. *Earth Planet. Sci. Lett.*, **55**, 171-180.

Manuscript received July 28, 2005.
Revised manuscript accepted December 20, 2005.